ACES Asian Chemical Editorial Society

doi.org/10.1002/asia.202500511

CHEMISTRY
AN ASIAN JOURNAL
Research Article

www.chemasianj.org

Confined RuP_2 Nanoparticles in N,P,S-Tridoped Carbon as Superior Electrocatalyst for pH-Wide Hydrogen Evolution

Yu Sun,[a] Haibo Li,[a] Suyuan Zeng,[a] Rui Li,[a] Qingxia Yao,[a] Hongyan Chen,[a] Yinghua Wang,*[b] Konggang Qu,*[a] and Lijian Meng*[c]

Hydrogen has been deemed as the ideal energy source and carrier due to its unmatched energy efficiency and sustainability. Nevertheless, there is a pressing need to develop cost-effective materials to replace costly Pt in the hydrogen evolution reaction (HER), and the electrocatalysts with low overpotential and robust stability under various conditions is a particularly significant concern. In this study, a straightforward and effective approach was proposed for the precise synthesis of RuP_2 nanoparticles encapsulated in N, P, S-tridoped carbon, which involves utilizing zinc pyrithione, phytic acid and Ru salt as starting materials. The effect of different Ru loadings on the morphology and structures of the composite catalysts was examined carefully. The obtained composites exhibit superior alkaline activity surpassing commercial Pt/C and comparable acidic and neutral activity as well as excellent pH-wide stability. DFT computations reveal the integration of RuP_2 with tridoped carbon can tailor the electronic structure of Ru active sites by interfacial electron transfer, thus optimizing the adsorption energy and promoting the HER activity. The benign graphitization of doped carbon and porous structures ensure the smooth charge and mass transfer during HER process. The cost-effective and straightforward synthesis methods presented in this work offer a promising alternative to commercial Pt/C for practical hydrogen-related applications.

1. Introduction

Hydrogen, as a clean energy carrier, has garnered significant attention owing to its remarkable attributes, including zero carbon emissions, high combustion enthalpy, and abundant availability.[1] Water electrolysis powered with renewable energy is considered as most promising to fulfill large-scale hydrogen production.[2] The employment of electrocatalyst materials is prerequisite to reduce the energy expenditure.[3] The electrocatalytic hydrogen evolution reaction (HER) can be conducted under varied conditions tailored to specific purposes.[4] Normally, the acidic HER can perform with highest kinetics but the highly corrosive conditions would degenerate or even decompose electrocatalysts, especially transition metal based catalysts.[5] The alkaline HER seems more acclaimed due to the relatively better stability of metal-based catalysts and the easier oxygen evolution in alkaline environments.[6,7] Furthermore, neutral water electrolysis allows for the direct utilization of seawater and can integrate with biocompatible microbial electrolysis cells.[8,9] Although alkaline and neutral HER can enable water electrolysis more flexible and provide more opportunities to select electrocatalysts, they still suffer from sluggish reaction kinetics associated with the slow water dissociation process.[10] To tackle these challenges, it is crucial to investigate electrocatalysts that are both highly efficient and stable across a wide range of pH conditions, essential for advancing hydrogen technology in practical applications.

In recent years, research has focused on investigating nonmetallic carbon and transition metal materials as substitutes for the rare and valuable platinum (Pt) in HER electrocatalysis.[11–13] However, the catalytic activity of reported carbon materials remains considerably lower compared to Pt/C.[14] Although only a few transition metal materials have been reported to exhibit activity comparable to or better than Pt/C,[15,16] their long-term stability in corrosive electrolytes remains a challenge.[17] Ruthenium (Ru), a member of the platinum group metals, shares similar properties with Pt, including an intrinsic anticorrosive property.[18–21] More importantly, these materials offer a cost advantage, being approximately 1/3 of the cost of Pt. Additionally, ruthenium phosphides like RuP and RuP_2 have demonstrated effective catalytic activity for the HER.[22,23] In these materials, doped carbons as substrates play vital roles, including dispersing and anchoring the catalysts, as well as tailoring the electronic properties of the metal species, thereby improving the apparent HER activity.[24,25] Although some researches about ruthenium phosphides have been reported for different application including but not limited to electrocatalysts, some

[a] Y. Sun, H. Li, S. Zeng, R. Li, Q. Yao, H. Chen, K. Qu
School of Chemistry and Chemical Engineering, Shandong Provincial Key Laboratory/Collaborative Innovation Center of Chemical Energy Storage & Novel Cell Technology, Liaocheng University, Liaocheng 252059, China
E-mail: qukonggang@lcu.edu.cn

[b] Y. Wang
College of Chemistry and Chemical Engineering, Dezhou University, Dezhou 253023, China
E-mail: wangyinghua@dzu.edu.cn

[c] L. Meng
Centre of Innovation in Engineering and Industrial Technology, Instituto Superior de Engenharia do Porto, Instituto Politecnico do Porto, Porto 4249-015, Portugal
E-mail: ljm@isep.ipp.pt

Supporting information for this article is available on the WWW under https://doi.org/10.1002/asia.202500511

contradictions still exist and should be addressed in detail. For example, the influence of metallic mass loading and particle size on the electrocatalytic performance need to be systematically investigated.[26,27] Additionally, integrating metal phase with carbon shells doped with multiple heteroatoms including N, P, and S remains infrequent, in which the multi-doped carbon may more robustly anchor the metal phase, possibly improve the catalytic durability in various conditions.[28,29] Meanwhile, the identification of active sites and the regulation of active centers by multi-doped carbon should be further appraised.[30,31] These efforts collectively aim to overcome current limitations and pave the way for the next generation of high-performance catalyst materials.

Previously, we prepared N, P, S-tridoped carbon (NPSC) for bifunctional ORR and HER using zinc pyrithione (ZPT) and phytic acid (PA) as precursors.[32] Although NPSC has attractive physical properties and superior ORR performance, it's HER activity still has a large gap with commercial Pt/C. Herein, Ru salt was introduced into the aforesaid system by simple mixing and pyrolysis, the RuP_2/N,P,S-tridoped carbon (RuP_2/NPSC) composite materials were obtained in which RuP_2 nanoparticles were encapsulated in N,P,S-tridoped carbons. The optimized RuP_2/NPSC has large surface area, mesoporous structures, high level of graphitization and abundant dopants, and resultantly exhibits better alkaline HER activity than commercial Pt/C as well as Pt-like activity in acidic and neutral electrolytes. The theoretical calculations reveal the interplay between RuP_2 and NPSC regulates the electronic property of Ru active sites located at the interface of RuP_2/NPSC composite and optimizes the H adsorption of Ru active sites, thereby leading to the enhanced HER activity.

2. Experimental Section

A mixture of ZPT and PA was added in absolute ethanol at a molar ratio of 1:2, after stirring for 2 h, different amount of $RuCl_3 \cdot xH_2O$ with the molar ratio of PA and Ru (1:0.2, 1:0.4, and 1:0.8) was added and continue to react for overnight with stirring. With drying by rotary evaporation, the collected mixture was subjected to pyrolysis in a tube furnace under an argon atmosphere at 900 °C for 2 h, with a heating rate of 5 °C min^{-1}. Afterward, the obtained material was washed three times with 0.5 M HCl. The RuP_2/NPSC composites contain 13.0, 19.2, and 59.2 wt% of Ru determined with inductively coupled plasma optical emission spectrometer (ICP-OES), denoted as RuP_2/NPSC-13.0%, RuP_2/NPSC-19.2%, RuP_2/NPSC-59.2%, respectively. The NPSC as the control sample was prepared using the same procedure described above, excluding the addition of Ru salt.

Details on catalyst characterization methods as well as electrochemical measurements can be found in the Supporting Information.

3. Results and Discussion

Scheme 1 illustrates the straightforward preparative route of RuP_2/NPSC composite. The powder X-ray diffraction (XRD) was first employed to identify the composition of metal in the freshly prepared catalysts. Noticeably, Figure 1A shows all the three catalysts share the same crystal structure, specifically, the distinct diffraction peaks observed at 23.0°, 30.4°, 35.8°, 47.5°, 50.2°, and 56.3° corresponding to the (110), (020), (101), (121), (211), and (310) crystal planes of RuP_2 (JCPDS No.34—0333), respectively.[33] The carbon skeleton information was studied using Raman spectroscopy (Figure 1B), where the ratio of intensities between the D band and the G band (I_D/I_G) reflects the presence of defects and disorder. Noteworthily, the smallest I_D/I_G value (0.88) was observed for RuP_2/NPSC-19.2% compared with that of RuP_2/NPSC-13.0% (0.95), RuP_2/NPSC-59.2% (1.00), and NPSC (0.97), indicating the best graphitic degree of RuP_2/NPSC-19.2%, which assures the good electrical conductivity for an electrocatalyst. The observed highest graphitic agree of RuP_2/NPSC-19.2% may be promoted with the moderate amounts of metal species, while excessive metal would possibly interrupt the continuous graphitic domains, leading to more disordered structures and defects in RuP_2/NPSC-59.2%. The specific surface area and pore structure of the newly prepared catalysts were investigated by the N_2 adsorption–desorption isotherms (Figure 1C and Figure S1A). The obtained isotherms are in good agreement to the type IV isotherms, indicating that the presence of the mesoporous structures. The Brunauer–Emmett–Teller (BET) surface area of RuP_2/NPSC-19.2% reaches an impressive 151.5 m^2/g, accompanied by a pore volume of 0.098 cm^3/g (Table S1), which notably exceeds that of RuP_2/NPSC-13.0% (63.8 m^2/g and 0.033 cm^3/g) and RuP_2/NPSC-59.2% (74.9 m^2/g and 0.058 cm^3/g). From the pore size distribution plot (Figure 1D and Figure S1B), it is evident that all three RuP_2-based catalysts and NPSC possess distinct mesoporous structures with average pore sizes of 3.3, 3.6, 4.4, and 3.4 nm. Importantly, these RuP_2-based catalysts exhibit much smaller surface areas and pore volumes compared to the metal-free NPSC (711.6 m^2/g and 0.38 cm^3/g), reflecting the successful incorporation of metal components into the carbon framework.[34]

The morphologies and microstructures of the newly-prepared catalysts were first examined by TEM. The typical TEM images (Figure 2, Figures S2 and S3) show that the three catalysts possess clear and dense nanoparticles with different sizes dispersed on ultrathin carbon sheets, the inset in Figure 2A indicates the nanoparticles are encapsulated by the distinct carbon layer. Moreover, the high-resolution transmission electron microscopy (HRTEM) reveals distinct lattice fringes at intervals of 0.383, 0.249, 0.230, and 0.178 nm (Figure 2B, Figures S2B and S3B), which correspond to the RuP_2 crystal planes of (110), (101), (121), and (211), respectively. These are also indicated in the selected-area electron diffraction (SAED) patterns (Figure 2C, Figures S2C and S3C) and match the XRD pattern's most prominent peaks at the specified angles.[35] The TEM elemental mapping images further validate the uniform distribution of elements C, N, O, and S, while the overlapping of P and Ru signals also suggest the formation of phosphide particles (Figure 2D, Figures S2D–I and S3D–I). Apparently, due to the different metal loading, RuP_2 nanoparticles have the average sizes of 5.5, 13.2, and 32.0 nm on the three catalysts (Figure 2E).

The elemental components in catalysts were then determined and analyzed accurately with XPS (Figure 3, Figures S4 and S5) and the quantitative information for the different elements

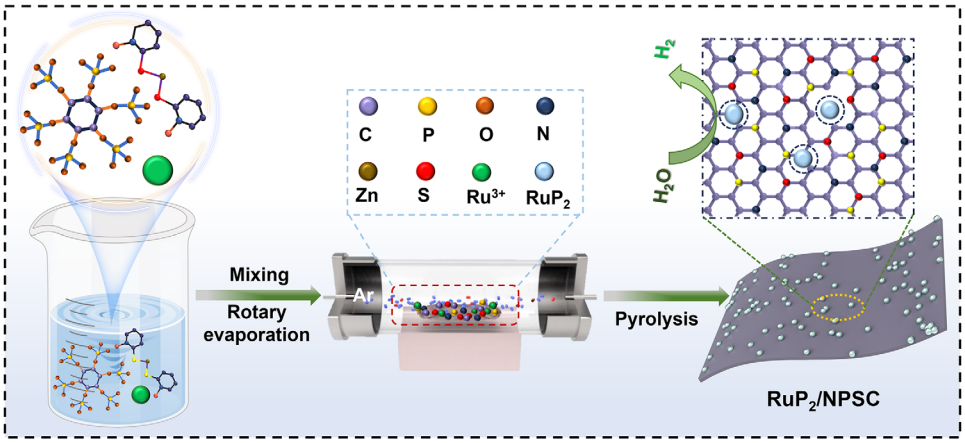

Scheme 1. Schematic preparation route of the RuP_2/NPSC composite by simple mixing and pyrolysis.

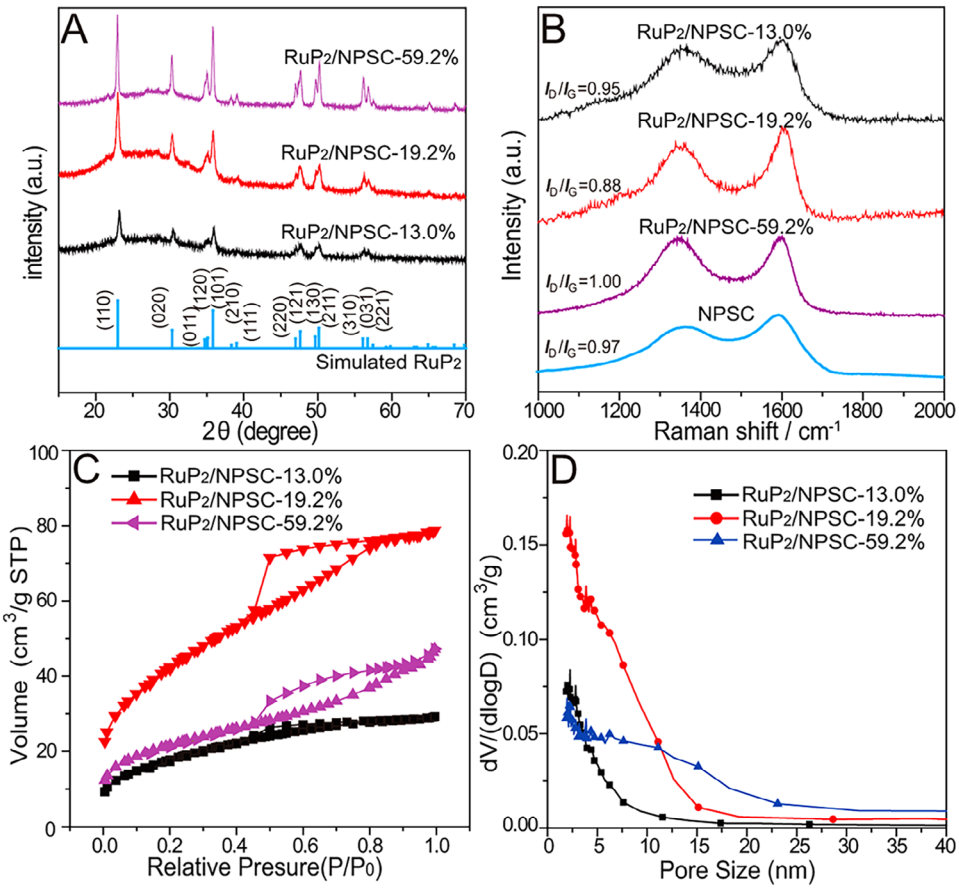

Figure 1. (A) XRD patterns, (B) Raman spectra, (C) N_2 adsorption–desorption isotherms, and (D) the pore size distribution curves.

was summarized in Table S2. XPS survey scan demonstrates the presence of N (3.05 at%), P (11.6 at%), S (3.33 at%), and Ru (3.45 at%) in RuP_2/NPSC-19.2% (Figure 3A). The high-resolution N 1s spectrum (Figure 3B) reveals four subpeaks around 398.7, 399.9, 401.2, and 404.4 eV, corresponding to different nitrogen functionalities in RuP_2/NPSC-19.2% including pyridinic N, pyrrolic N, graphitic N, and oxidized N, respectively.[36] Furthermore, the P 2p spectrum (Figure 3C) shows four discernible peaks: two at approximately 128.4 and 129.3 eV, which are consistent with the P $2p_{3/2}$ and P $2p_{1/2}$ states within the RuP_2 component, and two others centered around 133.2 and 134.4 eV, attributed to the P—C and P—O bonds, indicating effective P doping into the carbon matrix.[37] The deconvoluted S 2p peaks (Figure 3D) correspond to the S $2p_{3/2}$ (163.5 eV) and S $2p_{1/2}$ (164.8 eV) species of C—S—C.[38] Figure 3E illustrates the XPS region of Ru 3d, which overlap with C 1s post high-resolution deconvolution. A

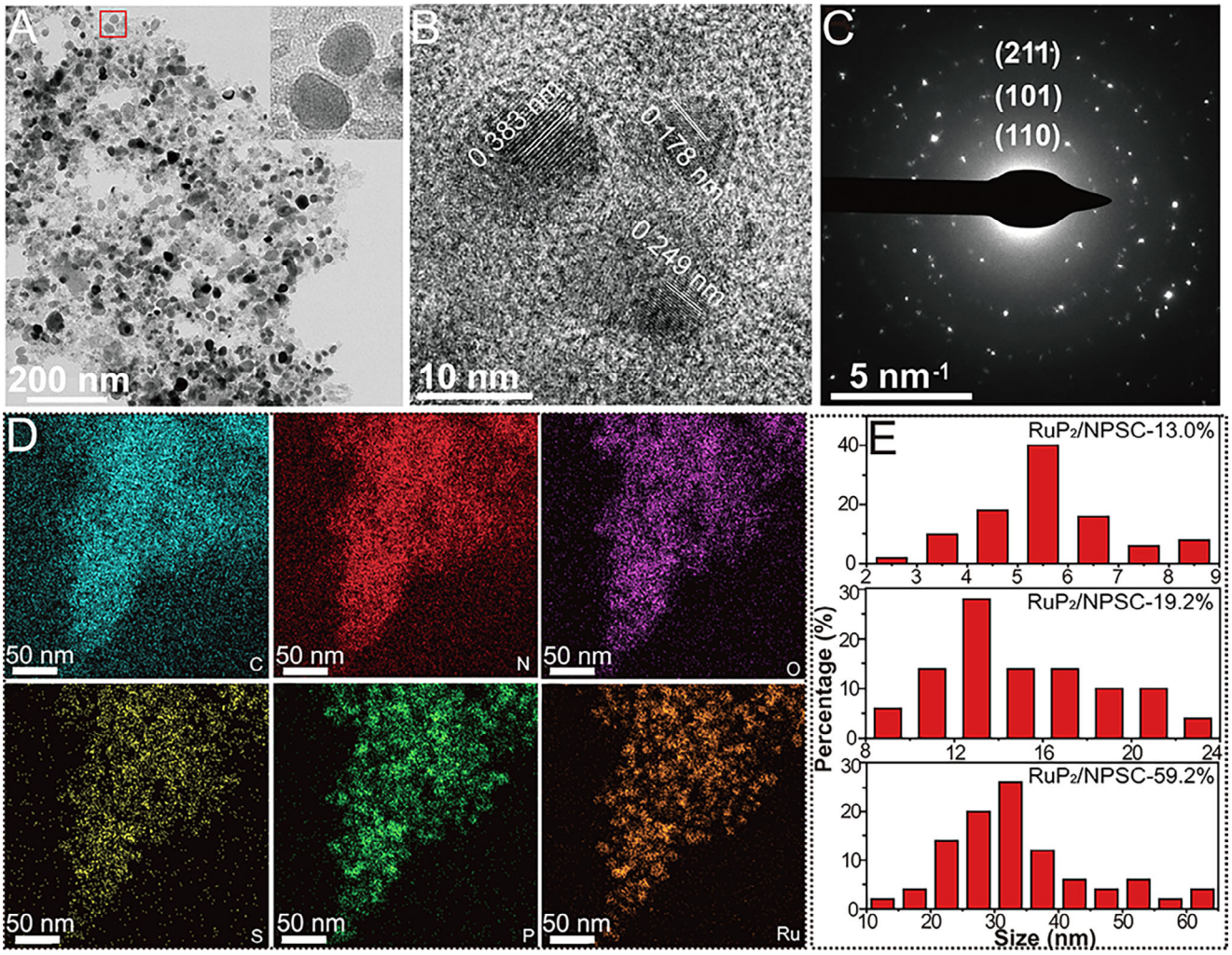

Figure 2. (A) TEM and (B) the high-resolution TEM images, (C) the SAED pattern and (D) TEM elemental mapping images of C, N, O, P, S, and Ru of RuP_2/NPSC-19.2%, and (E) the corresponding particle size distribution histograms of three RuP_2-based catalysts.

singular peak observed at 280.2 eV corresponds to Ru $3d_{5/2}$, accompanied by the Ru $3d_{3/2}$ peak centered at 284.4 eV, which suggests the presence of single RuP_2 component,[26] meanwhile, the peaks at 284.3, 285.3, 286.3, 287.5, and 288.9 eV are attributed to C═C, C—N/C—S, C—O/C—P, C═O, and COOH, respectively.[39,40] Additionally, the XPS spectrum of Ru 3p (Figure 3F) reveals two single peaks at 461.4 eV and 483.8 eV, corresponding to Ru $3p_{3/2}$ and Ru $3p_{1/2}$, further confirming the pure RuP_2 component.[41,42] Additionally, a large amount of O (13.7 at%) was found in RuP_2/NPSC-19.2% and would render the surface of catalyst hydrophilic, which can facilitate the catalyst/electrolyte interfacial contact and the subsequent evolution of H_2 gas.[43]

The HER electrocatalytic activity was first measured employing a typical three-electrode system in 1 M KOH. Commercial 20 wt% Pt/C, three RuP_2-based catalysts and the carbon counterpart NPSC were evaluated for comparative purposes. Figure 4A shows the linear scan voltammetry (LSV) curves. To generate a current density of 10 mA cm^{-2}, RuP_2/NPSC-19.2% exhibits an overpotential of only 19 mV, significantly lower than NPSC-RuP_2-13.0% (147 mV), NPSC-RuP_2-59.2% (111 mV), and NPSC (246 mV), matching that of Pt/C (19 mV), acting as the most active catalyst among all Ru-based catalysts (Table S3). Notably, NPSC-RuP_2-19.2% demonstrates a current density of 15 mA cm^{-2} at an overpotential of 30 mV, which exceeds the performance of Pt/C. Extraordinarily, RuP_2/NPSC-19.2% achieves a current density of 200 mA cm^{-2} at an overpotential of 125 mV, significantly outperforming Pt/C (265 mV), indicating superior high-current-density performance compared to Pt/C. Additionally, the obtained Tafel slope (Figure 4B) of RuP_2/NPSC-19.2% is 62 mV dec^{-1}, smaller than that of RuP_2/NPSC-13.0% (112 mV dec^{-1}), RuP_2/NPSC-59.2% (123 mV dec^{-1}), NPSC (86 mV dec^{-1}), and even Pt/C (66 mV dec^{-1}), manifesting the RuP_2/NPSC-19.2% catalyst has significant HER kinetics. Moreover, the Tafel slope values point to the possibility that the HER on RuP_2/NPSC-19.2% is dominated by the Volmer–Heyrovsky route, with the Heyrovsky reaction serving as the step that dictates the reaction rate, which is indicative of the electrochemical desorption process involving a hydrogen atom that has been chemically adsorbed and H_2O.[44,45] Further insights into the electrical conductivity of the catalysts were obtained through electrochemical impedance spectroscopy (EIS)

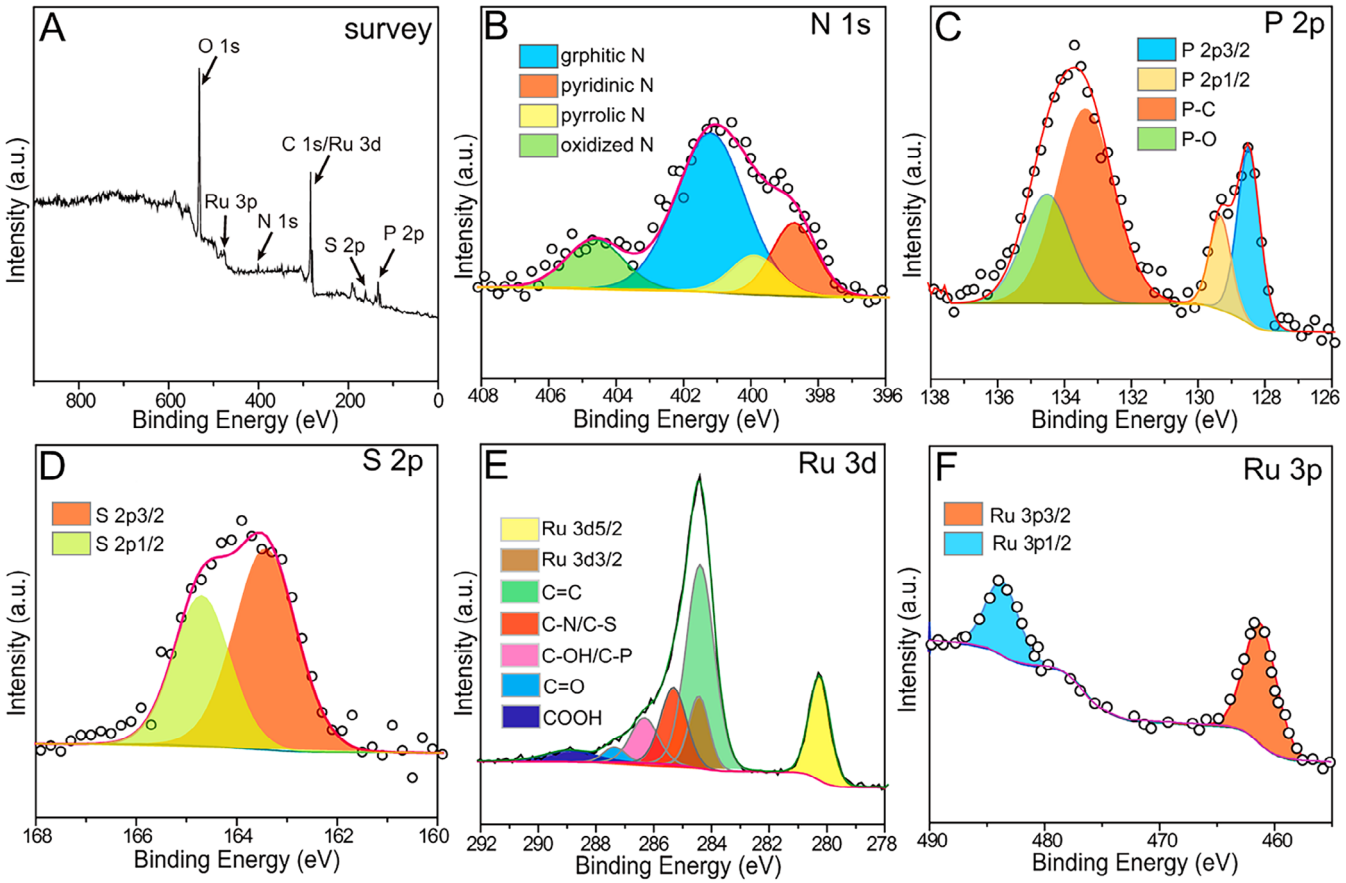

Figure 3. (A) XPS survey scan and high-resolution XPS spectra of (B) N 1s, (C) P 2p, (D) S 2p, (E) Ru 3d, and (F) Ru 3p of RuP_2/NPSC-19.2%.

measurements (Figure 4C). the electrocatalyst RuP_2/NPSC-19.2% exhibits the lowest charge transfer resistance (2.1 Ω) compared to RuP_2/NPSC-13.0% (10.8 Ω), RuP_2/NPSC-59.2% (9.7 Ω), and NPSC (13.6 Ω).

The capacity of the electrochemical double-layer (C_{dl}) is a measure that can be used to evaluate the electrochemically active surface areas (ECSA) due to their proportional relation.[20] As indicated in Figure 4D and Figure S6, the C_{dl} for RuP_2/NPSC-19.2% is recorded at 11.8 mF cm^{-2}, surpassing the values of 4.6 mF cm^{-2} for RuP_2/NPSC-13.0% and 5.5 mF cm^{-2} for RuP_2/NPSC-59.2%, although it is considerably less than the 36.9 mF cm^{-2} of NPSC. This aligns with the trends observed in BET surface areas and underscores that the active sites are predominantly associated with the RuP_2 phase rather than the doped carbon. RuP_2/NPSC-19.2% obviously has the most exposed active sites according to the BET surface area and C_{dl} analyses among RuP_2-based catalysts, which indeed favors the improvement of apparent HER activity. In addition, Figure 4E shows the LSV curves normalized to their ECSA, and RuP_2/NPSC-19.2% requires an overpotential at 25 mV for driving 1 mA cm^{-2}_{ECSA}, which is significantly lower than that of RuP_2/NPSC-13.0% (114 mV) and RuP_2/NPSC-59.2% (79 mV), meanwhile, RuP_2/NPSC-19.2% also has the best mass activity among three Ru-based catalysts and Pt/C (Figure 4F), these confirming the surface active sites of RuP_2/NPSC-19.2% has the highest intrinsic activity.[46,47] Furthermore, turnover frequency (TOF) was also calculated to evaluate the intrinsic unit activity for electrocatalytic HER (Figure 4G), specifically, the TOF value of RuP_2/NPSC-19.2% surpasses Pt/C from the overpotential of 70 mV and reaches 3.96 H_2 s^{-1} at 0.15 V, markedly higher than that of RuP_2/NPSC-13.0% (0.21 H_2 s^{-1}), RuP_2/NPSC-59.2% (0.08 H_2 s^{-1}), and even Pt/C (2.01 H_2 s^{-1}), indicating the superior intrinsic unit activity of RuP_2/NPSC-19.2%.[48,49] The stability was then evaluated with the accelerated durability testing (ADT) and amperometric I-t sweeps (Figure 4H,I). No clear activity degeneration of RuP_2/NPSC-19.2% is found after 1000 cyclic voltammetry sweeps. Additionally, a steady high current density can be achieved during the 50 h long-term measurement without observing any obvious decay. The XRD and TEM characterizations after the durability tests suggest the original RuP_2 crystalline structure in RuP_2/NPSC-19.2% is still maintained, underlining its excellent structural robustness (Figure S7).

The acidic and neutral HER performance was also tested in 0.5 M H_2SO_4 and 1.0 M phosphate buffered saline (PBS, pH = 7).[50,51] As shown in Figure 5A, to achieve a current density of 10 mA cm^{-2} in 0.5 M H_2SO_4, RuP_2/NPSC-19.2% demands an overpotential of 69 mV, which is considerably less than that of RuP_2/NPSC-13.0% (203 mV), RuP_2/NPSC-59.2% (214 mV), and NPSC (269 mV), and is just 15 mV lower than that of Pt/C

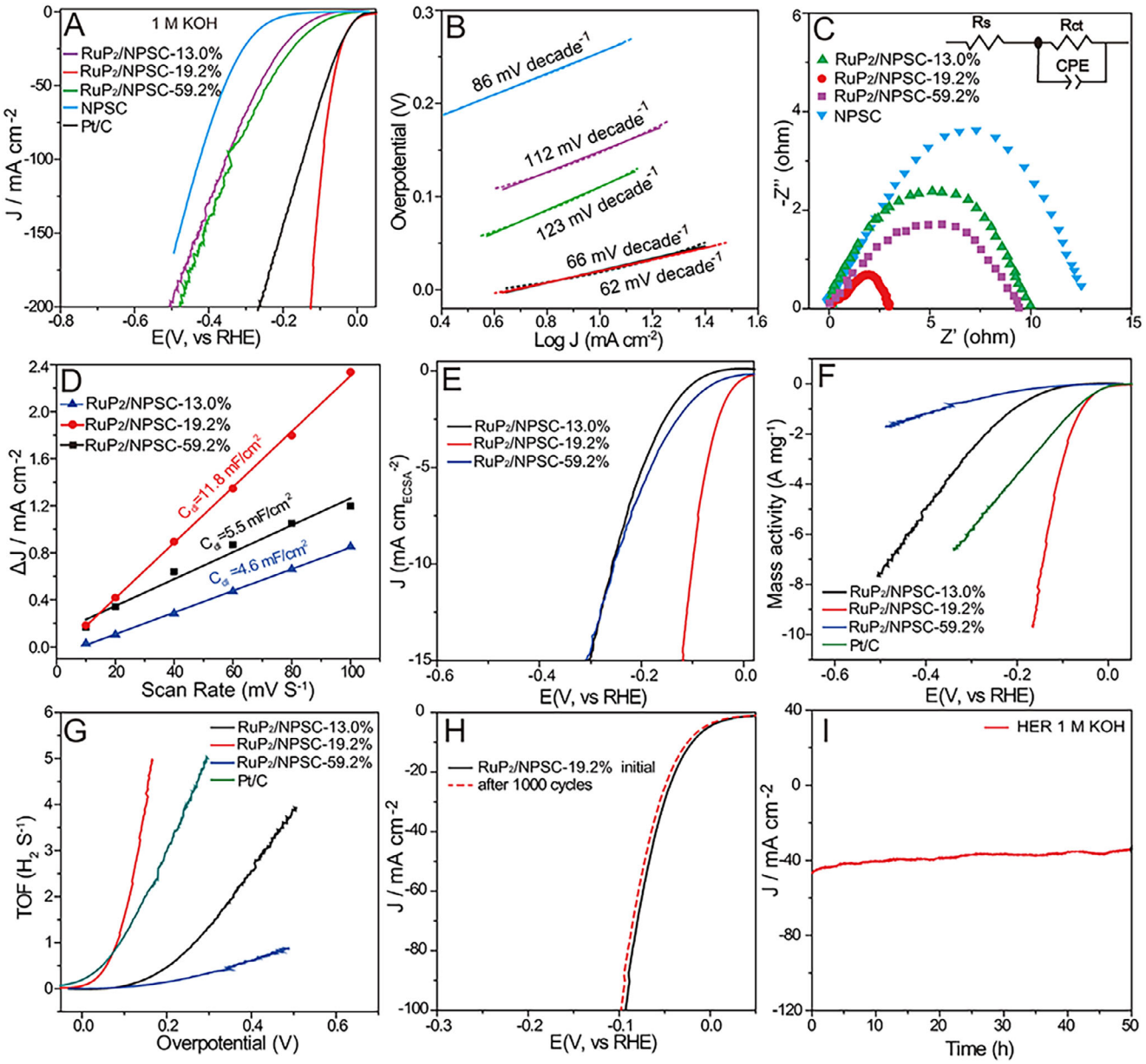

Figure 4. (A) HER LSV curves. (B) Tafel slopes. (C) EIS curves. (D) The calculated C_{dl} values of different catalysts. (E) LSV curves of three RuP_2-based samples normalized to their ECSA in 1 M KOH. (F) The mass activity of different samples for alkaline HER. (G) TOF values of three RuP_2-based samples with Pt/C in 1 M KOH. (H) LSV curves recorded before and after 1000 potential sweeps. (I) The long-time stability test of RuP_2/NPSC-19.2% in 1 M KOH.

(44 mV). At the same time, the Tafel slope of RuP_2/NPSC-19.2% is significantly lower at 48 mV dec^{-1} (Figure 5B), compared to RuP_2/NPSC-13.0% (124 mV dec^{-1}), RuP_2/NPSC-59.2% (135 mV dec^{-1}), and NPSC (113 mV dec^{-1}), and it closely resembles that of Pt/C (31 mV dec^{-1}). Figure 5C demonstrates that the catalyst's performance remains consistent before and after 1000 voltammetric cycles and also after a 50-h endurance test for acidic HER. Similarly, to achieve a current density of 10 mA cm^{-2} in 1.0 M PBS, NPSC-RuP_2-19.2% exhibits an overpotential of 68 mV (Figure 5D), outperforming RuP_2/NPSC-13.0% with 159 mV, RuP_2/NPSC-59.2% with 123 mV, NPSC with 427 mV, and nearly matching the performance of Pt/C at 10 mV. Furthermore, the Tafel slope for the RuP_2/NPSC-19.2% is 66 mV $decade^{-1}$, outperforming RuP_2/NPSC-13.0% (94 mV dec^{-1}), RuP_2/NPSC-59.2% (88 mV $decade^{-1}$), and NPSC (208 mV dec^{-1}), and approaching 33 mV $decade^{-1}$ of Pt/C (Figure 5E). Additionally, RuP_2/NPSC-19.2% also maintain the good durability in neutral media (Figure 5F). Furthermore, the RuP_2/NPSC-19.2% electrocatalyst also has the smallest charge-transfer resistance among the newly-prepared materials, indicating the favorable HER kinetics (Figure S8). The XRD and TEM data also confirm the structural stability after the durability tests for acidic and neutral HER (Figure S9). Notably, according to the Tafel slope values, the HER processes in acidic and neutral conditions also follow the Volmer–Heyrovsky route with the Heyrovsky reaction as the rate-determining step, similar to that for alkaline HER. Thus, these results indicate that RuP_2/NPSC-19.2% exhibits

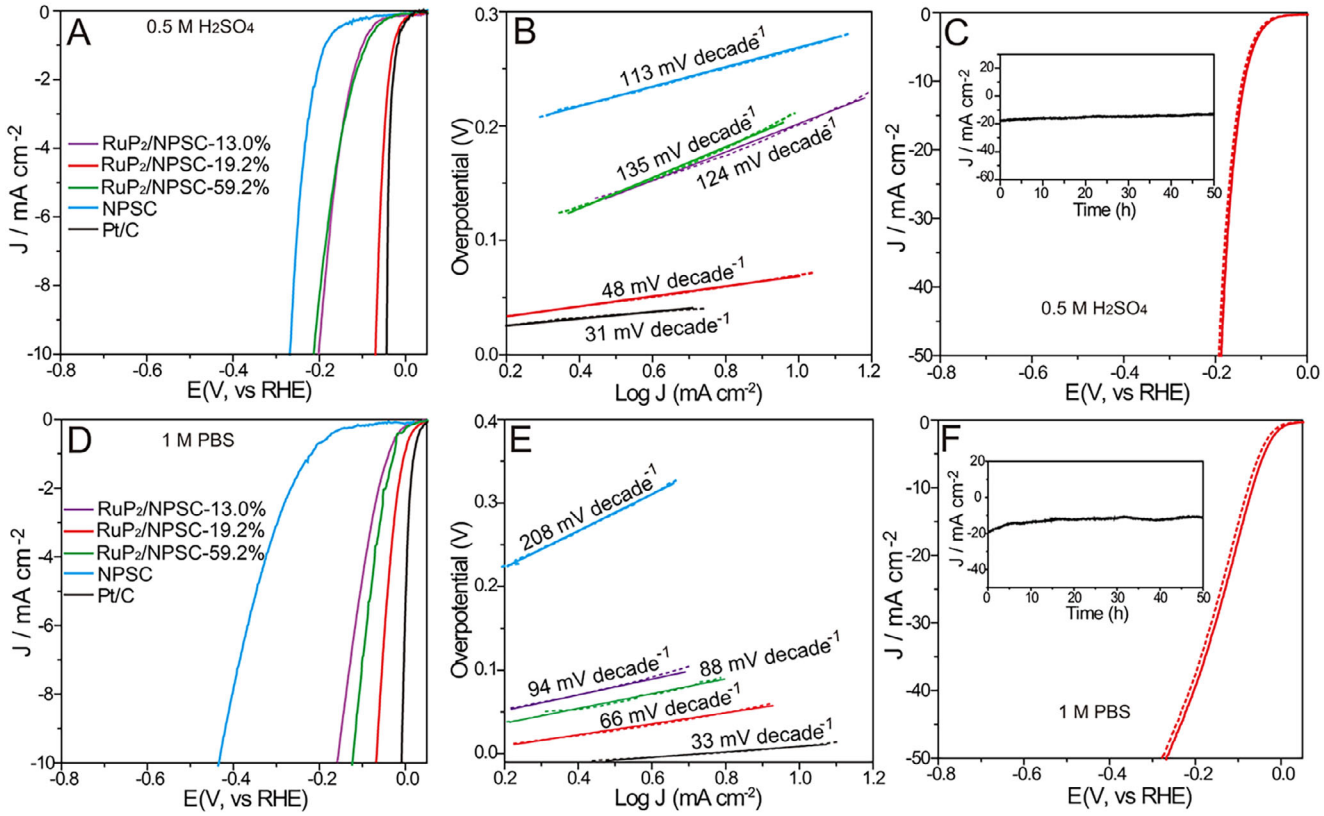

Figure 5. (A) HER LSV curves and (B) Tafel slopes of RuP_2/NPSC, NPSC, and Pt/C in 0.5 M H_2SO_4. (C) LSV curves recorded before and after 1000 potential sweeps and the long-time stability test of RuP_2/NPSC in 0.5 M H_2SO_4. (D) HER LSV curves and (E) Tafel slopes of RuP_2/NPSC, NPSC, and Pt/C in 1 M PBS. (F) LSV curves recorded before and after 1000 potential sweeps and the long-time stability test of RuP_2/NPSC in 1 M PBS.

excellent HER activity and stability in both acidic and neutral electrolytes.

To clearly decipher the fundamental origins of enhanced HER, DFT calculations were performed. According to the collected componential information, the structural models including N,P,S-tridoped graphene (NPSG), bare RuP_2 and RuP_2/NSPG composite were initially constructed as shown in Figure 6A, and RuP_2 (110) surface is energetically stable with strong reactivity and thus chosen as the active plane.[52–54] The cohesive energy of RuP_2/NPSG model was calculated to be −1.13 eV, suggesting the stability of composite structure. As for the optimal active sites of H* adsorption, several possible locations were considered on three different models (Figure S10). Specifically, on the NSPG model, the computations were performed on the S and P sites, which both have the positive values for free energy of hydrogen adsorption (ΔG_{H^*}) to be 1.77 and 0.45 eV, respectively (Figure S11A). While for the bare RuP_2, Ru site, and P site have very close ΔG_{H^*} values. Five possible sites were considered for the RuP_2/NSPG model, including P^1, P^2, Ru^1, Ru^2, and S sites (Figure S11B), and Ru^1 site, locating at the interface, where NSPG and RuP_2 interact, has the optimal ΔG_{H^*} value of 0.15 eV. Apparently, RuP_2/NSPG is more favorable to HER compared with NPSG and bare RuP_2, and the Ru site at the interface has the best HER activity (Figure 6B).

In order to thoroughly study the interplay between RuP_2 and NPSC for the improvement of HER performance, the differential charge density of RuP_2/NSPC was then examined. As shown in the inset of Figure 6C, the yellow and blue isosurfaces indicate high hole and high electron density, respectively, qualitatively confirming the distinct electron transfer at the interface between RuP_2 and NSPG, resulting in the interfacial charge redistribution. Additionally, the Bader charge and plane-averaged charge density at the RuP_2/NPSG interface were calculated to quantitatively investigate the interfacial charge transfer. Figure 6C shows that RuP_2 can transfer electrons of 0.31e to NPSG for RuP_2/NPSG model, and the plane-averaged charge density suggests the presence of a clear positive peak at the interface, while the charge density of RuP_2 at the interface was mainly negative.[55] Furthermore, the partial density of state (PDOS) and total density of states (TDOS) were computed for NPSG, bare RuP_2 and RuP_2/NPSG. As illustrated in Figure 6D, Figure S11C,D, the PDOS results of three models indicate that after RuP_2 binds to NSGP, the bandgap is significantly reduced and the conduction band moves downward, thus being more conducive for electron transfer in the HER process.

4. Conclusion

In conclusion, an uncomplicated method for creating RuP_2 nanoparticles confined in N,P,S-tridoped carbon was proposed by simple mixing and pyrolysis process. Ru loading was care-

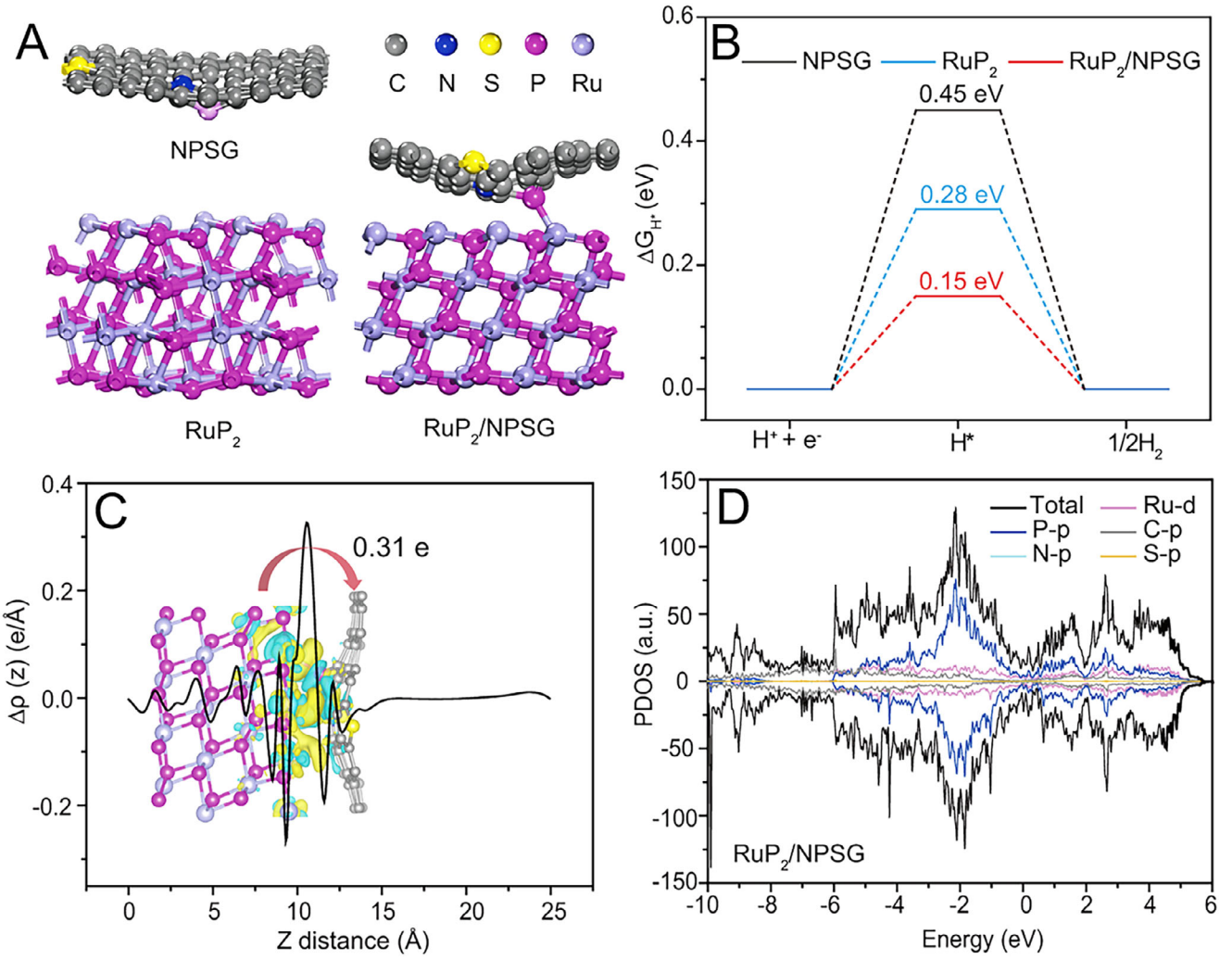

Figure 6. (A) The side-view structures of NSPG, bare RuP_2, and RuP_2/NSPG models. (B) The calculated adsorption energies of HER intermediate H* on NPSC, RuP_2, and RuP_2/NSPG. (C) The Bader charge and plane-averaged charge density at RuP_2/NSPG interface, with the inset showing the side view of differential charge density of RuP_2/NSPC, the yellow and cyan colors indicate charge accumulation and depletion, respectively, and the isovalue is 0.002 au. (D) The PDOS and TDOS of RuP_2/NSPG model.

fully examined to tailor the graphitization of tridoped carbon, surface area of catalyst and size of nanoparticles. The optimized RuP_2/NPSC-19.2% displays better alkaline HER activity than Pt/C and also comparable acidic and neutral HER activity. The RuP_2 nanoparticles confined by tridoped carbon afford the stable active sites for HER, and the tridoped carbon with high-level graphitization and large surface area endows the HER catalytic process with beneficial charge-transfer and mass-transfer ability. Theoretical calculations suggest that the integration of RuP_2 with doped carbon can modulate the electronic property of active Ru sites through interfacial electron transfer, thereby optimizing the adsorption energy and enhancing the performance for the HER.

Author Contributions

Yu Sun: Conceptualization; methodology; writing—original draft. **Haibo Li**: Conceptualization; formal analysis. **Suyuan Zeng**: Visualization; funding acquisition. **Rui Li**: Investigation; software. **Qingxia Yao**: Methodology; data curation. **Hongyan Chen**: Resources; project administration. **Yinghua Wang**: Supervision; project administration. **Konggang Qu**: Supervision; funding acquisition; writing—review and editing. **Lijian Meng**: Supervision; writing—review and editing.

Acknowledgements

This work was financially supported by the Development Project of Youth Innovation Team in Shandong Colleges and Universities (2019KJC031), Natural Science Foundation of Shandong Province (ZR2021MB122 and ZR2022MB137) and Doctoral Program of Liaocheng University (318051608).

Conflict of Interests

The authors declare no conflict of interest.

Data Availability Statement

The data that support the findings of this study are available from the corresponding author upon reasonable request.

Keywords: Electrocatalyst · Hydrogen evolution · pH-wide · RuP_2 · Tridoped carbon

[1] I. Staffell, D. Scamman, A. V. Abad, P. Balcombe, P. E. Dodds, P. Ekins, N. Shah, K. R. Ward, *Energy Environ. Sci.* **2019**, *12*, 463–491.
[2] S. Aralekallu, K. Sannegowda Lokesh, V. Singh, *Fuel* **2024**, *357*, 129753.
[3] Z. W. Seh, J. Kibsgaard, C. F. Dickens, I. Chorkendorff, J. K. Nørskov, T. F. Jaramillo, *Science* **2017**, *355*, eaad4998.
[4] W.-G. Cui, F. Gao, G. Na, X. Wang, Z. Li, Y. Yang, Z. Niu, Y. Qu, D. Wang, H. Pan, *Chem. Soc. Rev.* **2024**, *53*, 10253–10311.
[5] A. Parra-Puerto, K. L. Ng, K. Fahy, A. E. Goode, M. P. Ryan, A. Kucernak, *ACS Catal.* **2019**, *9*, 11515–11529.
[6] Y. Zhu, L. Li, H. Cheng, J. Ma, *JACS Au.* **2024**, *4*, 4639–4654.
[7] G. Gao, G. Zhu, X. Chen, Z. Sun, A. Cabot, *ACS Nano* **2023**, *17*, 20804–20824.
[8] C.-T. Dinh, A. Jain, F. P. G. de Arquer, P. De Luna, J. Li, N. Wang, X. Zheng, J. Cai, B. Z. Gregory, O. Voznyy, B. Zhang, M. Liu, D. Sinton, E. J. Crumlin, E. H. Sargent, *Nat. Energy* **2019**, *4*, 107–114.
[9] Z. Zhou, Z. Pei, L. Wei, S. Zhao, X. Jian, Y. Chen, *Energy Environ. Sci.* **2020**, *13*, 3185–3206.
[10] M. Lao, P. Li, Y. Jiang, H. Pan, S. X. Dou, W. Sun, *Nano Energy* **2022**, *98*, 107231.
[11] C. Hu, L. Dai, *Adv. Mater.* **2019**, *31*, 1804672.
[12] F. Islam, M. Ahsan, N. Islam, M. I. Hossain, N. M. Bahadur, A. Aziz, J. Y. Al-Humaidi, M. M. Rahman, T. Maiyalagan, M. A. Hasnat, *Chem. Asian J.* **2024**, *19*, e202400220.
[13] S. Hadimane, S. Aralekallu, L. K. Sannegowda, *Sustain. Energy Fuels* **2024**, *8*, 1775–1787.
[14] J. Liang, H. Li, L. Chen, M. Ren, O. A. Fakayode, J. Han, C. Zhou, *Ind. Crops Prod.* **2023**, *193*, 116214.
[15] H. Shi, Y.-T. Zhou, R.-Q. Yao, W.-B. Wan, X. Ge, W. Zhang, Z. Wen, X.-Y. Lang, W.-T. Zheng, Q. Jiang, *Nat. Commun.* **2020**, *11*, 2940.
[16] H. Xu, J. Wan, H. Zhang, L. Fang, L. Liu, Z. Huang, J. Li, X. Gu, Y. Wang, *Adv. Energy Mater.* **2018**, *8*, 1800575.
[17] Q. Ji, X. Yu, L. Chen, O. P. N. Yarley, C. Zhou, *Ind. Crops Prod.* **2021**, *172*, 114064.
[18] J. Mahmood, F. Li, S. Jung, M. S. Okyay, I. Ahmad, S. Kim, N. Park, H. Y. Jeong, J. Baek, *Nat. Nanotechnol.* **2017**, *12*, 441–446.
[19] X. Guan, Q. Wu, H. Li, S. Zeng, Q. Yao, R. Li, H. Chen, Y. Zheng, K. Qu, *Appl. Catal. B Environ.* **2023**, *323*, 122145.
[20] X. Guan, Y. Sun, S. Zhao, H. Li, S. Zeng, Q. Yao, R. Li, H. Chen, K. Qu, *SusMat* **2024**, *4*, 166–177.
[21] H. Li, W. Geng, X. Sun, W. Wei, X. Mu, W. Ahmad, M. M. Hassan, Q. Ouyang, Q. Chen, *Meat Sci.* **2021**, *177*, 108507.
[22] D. Li, R. Cai, D. Zheng, J. Ren, C.-L. Dong, Y.-C. Huang, S. J. Haigh, X. Liu, F. Gong, Y. Liu, J. Liu, D. Yang, *Adv. Sci.* **2024**, *11*, 2309869.
[23] H. Du, Z. Du, T. Wang, B. Li, S. He, K. Wang, L. Xie, W. Ai, W. Huang, *Adv. Mater.* **2022**, *34*, 2204624.
[24] I. C. Gerber, P. Serp, *Chem. Rev.* **2020**, *120*, 1250–1349.
[25] J. Li, X.-Y. Wang, B.-J. Zhu, Z. Zhou, K.-M. Pan, X.-M. Liu, Z.-L. Zhuang, Q.-B. Zhang, *Rare Met.* **2025**, *44*, 1411–1442.
[26] J. Yu, Y. Guo, S. She, S. Miao, M. Ni, W. Zhou, M. Liu, Z. Shao, *Adv. Mater.* **2018**, *30*, 1800047.
[27] Q. Qin, H. Jang, L. Chen, G. Nam, X. Liu, J. Cho, *Adv. Energy Mater.* **2018**, *8*, 1801478.
[28] Y. Jiang, L. Du, W. Sun, Q. Zhang, Y. Su, M. Sun, G. Yin, *Int. J. Hydrogen Energy* **2024**, *51*, 725–732.
[29] Y.-H. Wang, R.-Q. Li, H.-B. Li, H.-L. Huang, Z.-J. Guo, H.-Y. Chen, Y. Zheng, K.-G. Qu, *Rare Met.* **2021**, *40*, 1040–1047.
[30] Z. Y. Yu, Y. Duan, X. Y. Feng, X. Yu, M. R. Gao, S. H. Yu, *Adv. Mater.* **2021**, *33*, 2007100.
[31] B. Singh, T. Ansari, A. Indra, *Chem. Asian J.* **2025**, *20*, e202401484.
[32] Y. Wang, S. Wang, R. Li, H. Li, Z. Guo, B. Chen, R. Li, Q. Yao, X. Zhang, H. Chen, Y. Li, K. Qu, Y. Zheng, *Carbon* **2020**, *162*, 586–594.
[33] Q. Chang, J. Ma, Y. Zhu, Z. Li, D. Xu, X. Duan, W. Peng, Y. Li, G. Zhang, F. Zhang, X. Fan, *ACS Sustainable Chem. Eng.* **2018**, *6*, 6388–6394.
[34] Q. Yu, H. Li, R. Li, S. Zeng, R. Li, Q. Yao, H. Chen, K. Qu, Y. Zheng, *Carbon* **2022**, *186*, 171–179.
[35] J. Wang, Q. Yu, H. Li, R. Li, S. Zeng, Q. Yao, Z. Guo, H. Chen, K. Qu, *Chem. Commun.* **2021**, *57*, 7284–7287.
[36] Y. Sun, L. Wang, H. Li, S. Zeng, R. Li, Q. Yao, H. Chen, K. Qu, *Carbon Neutralization* **2025**, *4*, e196.
[37] Y. Hong, S. C. Cho, S. Kim, H. Jin, J. H. Seol, T. K. Lee, J.-k. Ryu, G. M. Tomboc, T. Kim, H. Baik, C. Choi, J. Jo, S. Jeong, E. Lee, Y. Jung, D. Ahn, Y.-T. Kim, S. J. Yoo, S. U. Lee, K. Lee, *Adv. Energy Mater.* **2024**, *14*, 2304269.
[38] G. Liu, Y. Chen, Y. Chen, Y. Shi, M. Zhang, G. Shen, P. Qi, J. Li, D. Ma, F. Yu, X. Huang, *Adv. Mater.* **2023**, *35*, 2304716.
[39] Y. Li, S. Li, Y. Wang, J. Wang, H. Liu, X. Liu, L. Wang, X. Liu, W. Xue, N. Ma, *Phys. Chem. Chem. Phys.* **2017**, *19*, 11631–11638.
[40] K. Qu, Y. Wang, X. Zhang, H. Chen, H. Li, B. Chen, H. Zhou, D. Li, Y. Zheng, S. Dai, *ChemNanoMat* **2018**, *4*, 417–422.
[41] K.-G. Qu, Z.-F. Chen, L.-H. Wang, H.-B. Li, S.-Y. Zeng, R. Li, L.-J. Meng, H.-Y. Chen, Q.-X. Yao, *Rare Met.* **2025**, *44*, 2094–2102.
[42] J. Chen, Y. Ha, R. Wang, Y. Liu, H. Xu, B. Shang, R. Wu, H. Pan, *Nano-Micro Lett.* **2022**, *14*, 186.
[43] K. Qu, Y. Zheng, Y. Jiao, X. Zhang, S. Dai, S. Z. Qiao, *Adv. Energy Mater.* **2016**, *7*, 1602068.
[44] Y. Lin, K. Sun, S. Liu, X. Chen, Y. Cheng, W.-C. Cheong, Z. Chen, L. Zheng, J. Zhang, X. Li, Y. Pan, C. Chen, *Adv. Energy Mater.* **2019**, *9*, 1901213.
[45] R. Tang, Y. Yang, Y. Zhou, X.-Y. Yu, *Adv. Funct. Mater.* **2024**, *34*, 2301925.
[46] H. Yang, Z. Chen, P. Guo, B. Fei, R. Wu, *Appl. Catal. B Environ.* **2020**, *261*, 118240.
[47] J. Li, C. Zhang, C. Zhang, H. Ma, Y. Yang, Z. Guo, Y. Wang, H. Ma, *Chem. Eng. J.* **2022**, *430*, 132953.
[48] K. Wang, J. Zhou, M. Sun, F. Lin, B. Huang, F. Lv, L. Zeng, Q. Zhang, L. Gu, M. Luo, S. Guo, *Adv. Mater.* **2023**, *35*, 2300980.
[49] J. Wu, M. Liu, J. Fan, Y. Qiu, W. Lu, X. Fan, W. Zhang, L. Zhang, X. Cui, *Adv. Funct. Mater.* **2024**, *34*, 2409825.
[50] J. Zhou, Y. Xie, L. Yang, Y. Liu, Y. Du, L. Yu, Y. Yu, *Inorg. Chem. Front.* **2023**, *10*, 2842–2859.
[51] Q. Hu, J. Cao, S. Qi, N. Meng, J. Zhao, T. Huang, J. You, T. Liang, C. Shang, J. Yu, H. Yang, C. He, *Angew. Chem. Int. Ed. Engl.* **2025**, *64*, e202416402.
[52] Z. Pu, I. S. Amiinu, Z. Kou, W. Li, S. Mu, *Angew. Chem. Int. Ed. Engl.* **2017**, *56*, 11559–11564.
[53] T. Liu, J. Wang, C. Zhong, S. Lu, W. Yang, J. Liu, W. Hu, C. M. Li, *Chem.-A Eur. J.* **2019**, *25*, 7826–7830.
[54] Y. Li, J. Zhang, Y. Liu, Q. Qian, Z. Li, Y. Zhu, G. Zhang, *Sci. Adv.* **2020**, *6*, eabb4197.
[55] X. Guan, H. Li, R. Li, S. Zeng, R. Li, Q. Yao, H. Chen, Y. Zheng, K. Qu, *Carbon* **2022**, *195*, 123–130.

Manuscript received: March 24, 2025
Revised manuscript received: April 21, 2025
Version of record online: May 14, 2025